Open check dams and large wood: head losses and release conditions

Guillaume Piton[1], Toshiyuki Horiguchi[2], Lise Marchal[1,3], Stéphane Lambert[1]

[1]Univ. Grenoble Alpes, INRAE, ETNA, F-3800 Grenoble, France.
[2]National Defense Academy, Yokosuka, 239-8686, Kanagawa, Japan
5   [3]AgroParisTech, Paris Institute of Technology for Life, Food and Environmental Sciences, F-75231 Paris, France

Correspondence to: Guillaume Piton (guillaume.piton@inrae.fr)

Abstract.

10   Open check dams are strategic structures to control sediment and large wood transport during extreme flood events in steep streams and piedmont rivers. Large wood (LW) tends to accumulate against such structures, to obstruct their openings and to increase energy dissipation and thus, flow levels. To which extent open check dams' stage-discharge relationships are consequently modified by LW presence was not clear so far. This question is key (i) to estimate how much bedload transport might be trapped in the related backwater areas and (ii) to estimate how high is the overflowing depth atop the structure.

15   These flows, when sufficiently high, might trigger a sudden release of the previously trapped LW with eventual dramatic consequences downstream. This paper provides experimental quantification of LW-related energy dissipation and simple ways to compute the related increase in water depth at dams of various shapes: trapezoidal, slit, slot and SABO (i.e., made of piles), including flow capacity through their open body and atop the spillway. It was additionally observed that LW is often released over the structure when the overflowing depth, i.e., depth above the spillway, is about 3-5 the mean log diameter.

20   Two regimes of LW accumulations were observed: dams with low permeability generate low velocity upstream and LW then accumulates as floating carpets, i.e., as a floating single layer. Conversely, dams with high permeability maintain high velocities close to the dams and LW tends to jam them in dense complex 3D patterns because drag forces are stronger than buoyancy and logs are sucked below the flow surface. In such cases, LW releases occur for higher overflowing depth and LW-related head losses are higher. A new dimensionless number, namely the ratio buoyancy to drag force, enables to

25   compute whether or not flows stay in the floating carpet domain where buoyancy prevails.

Key words: woody debris; head losses; hyper-congested large wood transport; torrent control

1   Introduction

Open check dams, also called debris basins (Dodge, 1948), SABO dams (Ikeya, 1989; Mizuyama, 2008), torrential

30   barriers (Rudolf-Miklau and Suda, 2013) or debris racks (Schmocker and Hager, 2013), are key structures in the mitigation of hazards related to solid transport, i.e., sediment and large wood (Piton and Recking, 2016a, 2016b). Large wood, hereafter "LW", is defined as logs thicker than 0.1 m and longer than 1 m (Braudrick et al., 1997). Extreme flood events occurring in

forested catchments involve water, sediment but also LW (Ruiz-Villanueva et al., 2019). Although extreme flood events are first related to large amounts of water, LW might actually play a significant role in flood hazards by clogging bridges and

35   disturbing hydraulic structures, thus aggravating flooding and sediment deposition (Mazzorana and Fuchs, 2010; Mazzorana et al., 2009; Ruiz-Villanueva et al., 2014b; Schmocker and Weitbrecht, 2013, Chen et al., 2020). In rivers equipped with dams or bridges that are prone to be clogged by LW, it is thus required to either (i) adapt these structures to avoid the clogging or (ii) trap LW recruited during extreme floods before it reached the sensitive structures. Open check dams are relevant options to achieve this objective in torrents and piedmont rivers (Comiti et al., 2016; Wohl et al., 2016, 2019).

40   Open check dams aim at trapping all or part of sediment and/or LW during floods or debris flows (Hübl and Fiebiger, 2005). Scientific works aiming at better understanding how sediment may be trapped in open check dams are numerous (Armanini et al., 1991; Dodge, 1948; Ikeya, 1985; Reneuve, 1955; Zollinger, 1985), see the review of Piton and Recking (2016a). One key conclusion was that increased water depth at the dam passage, induces a low velocity area in the dam backwater where bedload might be trapped. Computing the stage-discharge relationship is thus a critical design step to assess sediment-

45   trapping efficacy.

Studies on interactions between LW and open check dams started more recently, in the late 1980s in Japan (Ishikawa and Mizuyama, 1988; Ishikawa, 1994; Kasai et al., 1996; SABO Division, 2000; Uchiogi et al., 1996), and later in the 2000s in Europe (Bezzola et al., 2004; D'Agostino et al., 2000; Lange and Bezzola, 2006). These works mostly focused on trapping efficacy and on defining relevant opening sizes and shape to achieve appropriate functioning. Numerical modelling of LW

50   freely floating or interacting with structures emerged in the 2010s and is in constant improvement (Horiguchi et al., 2015; Kimura and Kitazono, 2019; Ruiz-Villanueva et al., 2014a; Shrestha et al., 2012).

       Field observations complete these laboratory and numerical works: Bezzola et al. (2004) in particular reported examples of open check dams dysfunctions in presence of LW. They proposed options to adapt existing works notably by adding grills upstream of slit and slot dams. Shima et al. (2015, 2016) also reported key effects of LW presence in the

55   functioning of open check dams in Japan. The topic of interactions between LW and open check dams was reviewed by Piton and Recking (2016b). Two scientific questions in particular remained insufficiently covered: (i) how much LW increases energy dissipation and thus the flow level at a structure by obstructing the flow section? and (ii) which conditions drive the sudden downstream release of LW accumulated by the structure when the structure is overtopped, thus dramatically aggravating bridge jamming hazards?

60   The first question was yet addressed for reservoir dams: for ogee crest spillways with piles by Hartlieb (2012, 2017) and for piano-key weirs (PK-weirs) by Pfister et al. (2013b). It was also recently thoroughly covered by the hydraulic research team of ETH Zürich for rack structures made of piles (Schalko et al., 2018, 2019a, 2019b; Schmocker and Hager, 2013; Schmocker and Weitbrecht, 2013; Schmocker et al., 2014). Recent experiments by Rossi and Armanini (2019), Meninno et al. (2019) and Chen et al. (2020) also explored trapping efficacy of slits dams, without and eventually with upstream grills as

65   suggested by Bezzola et al. (2004). All these works describe comprehensively how LW accumulates against barriers. In addition, they proposed methods to compute head losses related to LW accumulating against racks. Despite the high

randomness of the processes, approaching flow conditions (e.g., Froude number, flow depth, water discharge) and features of the LW mixtures (LW volume, LW diameter, presence of fine material as branches and leaves) were demonstrated to drive LW-related head losses.

70 The second question of conditions of LW releases during overtopping was addressed only by authors working on reservoir dam spillways: Pfister et al. (2013a) for PK-weirs, as well as Furlan et al. (2018) and Furlan (2019) for ogee crests with piles. These works concluded that the ratio of flow depth to LW diameter was key to discriminate either LW stays in the reservoir or overtops the dam. The ratio of LW length to pile interval was also known from SABO and slit dam experiments (Ishikawa and Mizuyama, 1989, Horiguchi et al., 2015, Chen et al. 2020). Works on racks and slit dams did not address the

75 question of LW overtopping because the modelled structure were not overtopped (Schmocker and Hager, 2013; Schmocker and Weitbrecht, 2013; Schmocker et al., 2014, Schalko et al., 2018, 2019a, 2019b, Rossi and Armanini 2019, Meninno et al., 2019, Chen et al., 2020). The authors merely reported high trapping efficacy (>90%) for the tested racks and trapping efficacy varying with slit width and interval between upstream grill bars. It is consequently not clear which conditions drive the release of LW above open structures as SABO, slit, slot or trapezoidal dams. One could hypothesize that results from

80 dam reservoir spillways might be transferable to open check dams. However flow conditions upstream of open check dams, e.g., higher Froude number might partially modify the jamming and release processes.

Since water depth above the structure seems a key driver of both sediment trapping and LW release, this paper seeks first to provide a way to compute water depth at structures in presence of LW, and secondly to study conditions driving the release of the trapped elements. This paper explores both questions experimentally. It is organized in four sections and a conclusion:

85 hydraulic computation of water stage – discharge relationships is first presented, the experimental apparatus used is secondly described and results are thirdly presented and finally discussed. Throughout this paper, we try to consistently use the term "overflowing" when speaking about the water passing over the dam and rather "overtopping" when referring to the passage of LW.

2   Computing open check dam discharge capacity

90   Stage-discharge relationships were used according to the state-of-the-art (Piton and Recking, 2016a, 2016b). In addition, dimensionless coefficients called β_i (-) were introduced to account for the LW-related energy dissipation. The relationship between water depth with LW, noted h (m), water depth without LW noted h_0 (m), LW-related head loss noted Δh (m) and β_i is as follow (see notations in Figure 1):

$$h = h_0 + \Delta h = h_0 \left(1 + \frac{\Delta h}{h_0}\right) \quad \Leftrightarrow \quad h_0 = \frac{h}{\left(1+\frac{\Delta h}{h_0}\right)} \quad \underset{h \approx H}{\Longleftrightarrow} \quad \frac{\Delta h}{h_0} = \beta_i \qquad (1)$$

95 with $H = h+V^2/2g = h(1+Fr^2/2)$ the flow energy (m), V the flow velocity (m/s), g the gravitational acceleration (9.81 m/s²) and $Fr=V/(gh)^{0.5}$ the Froude Number (-). It is worth recalling that depth h should be replaced by energy H in stage-discharge relationships wherever the approximation $h \approx H$ is wrong (Piton et al., 2016), e.g., for $Fr> 0.3$ if one accepts a 5 %

difference on the hypothesis $h \approx H$. All runs with LW performed for the present paper are in the range $0.01 < F r < 0.3$; h is

thus used in stage-discharge relationships.
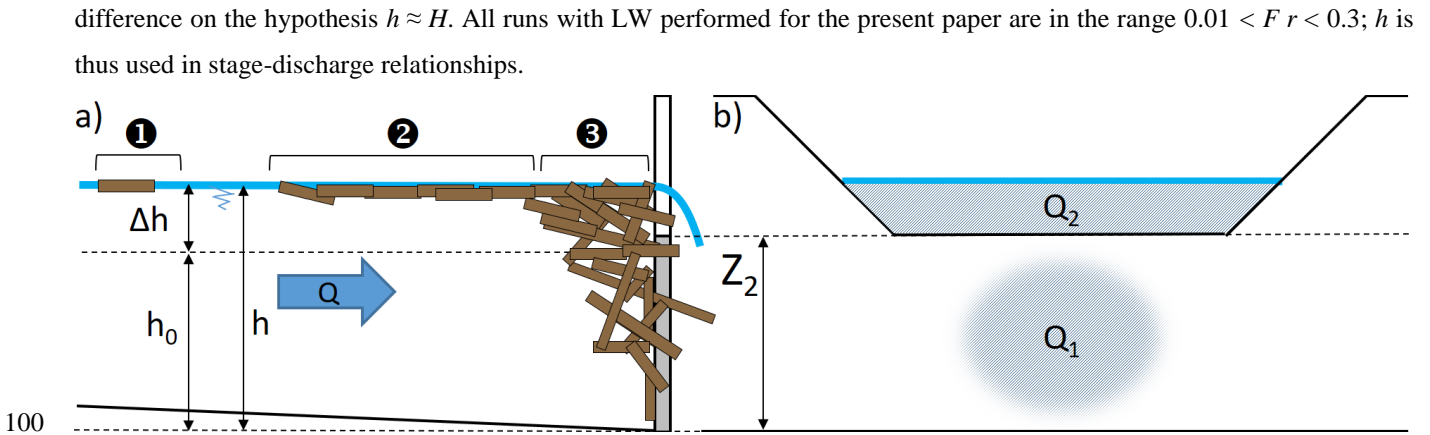
Figure 1. Notation used throughout the paper: a) side view of LW jamming a barrier and b) front view of barrier. Water depth without LW and with LW are noted h_0 and h, respectively. The difference between h and h_0 is the head loss Δh. Dam crest is of height z_2. Logs may be (1) freely flowing, (2) floating in a single layer as a carpet or (3) jamming the barrier with most pieces submerged. The total water discharge Q is split in Q_1 the discharge passing through the dam and Q_2 the discharge overflowing the dam

For the flow passing through the dams Q_1 (m³/s) , the Grand Orifice equation was used:

$$Q_1 = N\mu_1 W_1 \frac{2}{3}\sqrt{2g}\left(\left(\frac{h}{1+\beta_1}\right)^{1.5} - \left(\frac{h-h_1}{1+\beta_1}\right)^{1.5}\right) \tag{2}$$

Where N is the number of similar openings (-), μ_1 is the orifice coefficient (-), W_1 is the opening width (m), h_1 is the opening

height (m) and β_1 is a coefficient to account for LW-related head losses on discharge *passing through the dam* (-). If flow

depth h is lower than orifice height h_1, the second term is removed and the equation is a simple slit flow equation.

The spillway capacity Q_2 (m³/s) is computed using a trapezoid weir equation (Deymier et al., 1995, p.70):

$$Q_2 = \mu_2\left(W_2\sqrt{2g}\left(\frac{h-z_2}{1+\beta_2}\right)^{1.5} + \frac{0.8}{\tan\Phi}\sqrt{2g}\left(\frac{h-z_2}{1+\beta_2}\right)^{2.5}\right) \tag{3}$$

Where μ_2 is the weir coefficient (-), W_2 is the spillway horizontal width (m), z_2 is the spillway level (m), β_2 is another

coefficient to account for LW-related head losses *in flows overflowing the barrier* (-) and Φ is the angle between horizontal

and wing crest (45° in our experiments).

Coefficients β_i are set to zero in the absence of LW, the formulation then being the classical one. Using β_i=0.6 means

for example that compared to pure water flow, the flow depth will increase by 60 % to convey the same water discharge

through the LW accumulation over the same dam. Although it is quite similar, its reading and interpretation is more

straightforward than providing direct estimation of Δh (which is dimensional and discharge-specific) or modification of weir

or orifice coefficients as e.g., the 30% reduction proposed by CFBR (2013) for reservoir dam spillways, for which

computation is required to know the related stage increase. The dam total capacity Q (m³/s) is computed by summing Eqs.

(2) and (3).

$$Q = Q_1 + Q_2 = \mu_1 W_1 \frac{2}{3}\sqrt{2g}\left(\left(\frac{h}{1+\beta_1}\right)^{1.5} - \left(\frac{h-h_1}{1+\beta_1}\right)^{1.5}\right) + \mu_2\left(W_2\sqrt{2g}\left(\frac{h-z_2}{1+\beta_2}\right)^{1.5} + \frac{0.8}{\tan\Phi}\sqrt{2g}\left(\frac{h-z_2}{1+\beta_2}\right)^{2.5}\right) \tag{4}$$

It is worth noting that the Grand Orifice equation is used to compute discharge through the dam even for slit and SABO dams that are precisely not structures with orifices but rather gap-crested structures. For the gap-crested dams with slits, $h_1 = z_2$, i.e., the orifice height is the same than the slit height. Doing so, we compute separately the discharge passing through the dam Q_1 and the discharge overflowing the structure above the slit top in Q_2. We selected this option because the relative energy losses are bigger in flows over the structure (i.e., the one passing through the floating jam), than in flows passing through the structure (see later). In other words, logs floating, the energy dissipation is higher in the discharge over the weir than in discharge passing through the slit, i.e., $\beta_2 > \beta_1$.

3   Material and methods

3.1   Flume and sensors

The experimental setup is not a downscaled version of a particular site. It is somewhat representative of a 1:30 scale model and scales 1:20-1:40 remain relevant to the authors' opinion. Any upscaling should be performed using the Froude similitude. The experimental setup is presented more in detail in the research report of Piton et al. (2019b). The flume was 6.0 m long, 0.4 m wide and 0.4 m deep. Its adjustable slope was set at 0.02 m/m for all experiments. The tested dams were installed at the downstream end of the flume, perpendicular to its bottom. Flow depth was measured at a frequency of 10 Hz by an ultrasonic sensor located 20 cm upstream of dams. Water discharge was measured with an electronic flow meter. Water discharge was increased step by step. An automatic system adjusted pumps velocities to achieve the targeted discharge. Each water depth or discharge measurement provided in the following is computed as the mean value on a step lasting 1-4 minutes. These averaging time windows started when flow depth was stable after the transient period related to change from one discharge step to another, and stopped just before discharge changed again. Standard deviations of discharge and flow depth were also computed and later used as a proxy of the uncertainty on each measurement. Error bars are displayed on plots wherever uncertainties, computed after quadratic error propagation, were high enough such that error bars were bigger that dots. LW released during each step were weighted on a scale as well as the total LW sample at the end of each run. LW releases were arbitrarily considered as "significant" if the mass released during one step was more than 10% the weight of all LW used in the experiment.

3.2   Dams

A selection of the most common check dams encountered in France and Japan was tested (Horiguchi et al., 2015; Piton et al., 2019a): (i) closed-type dam figuring a check dam recently dredged, (ii) slit dams with horizontal grills, (iii) slot dams with five openings and (iv) SABO dams with 11 openings that could figure the widely used steel pipes dams very common in Japan. The shape and size of dams are provided in Figure 2. All dams have a crest set at $z_2 = 55$ mm. They were made of transparent Plexiglas plates, 10 mm thick and numerically cut.
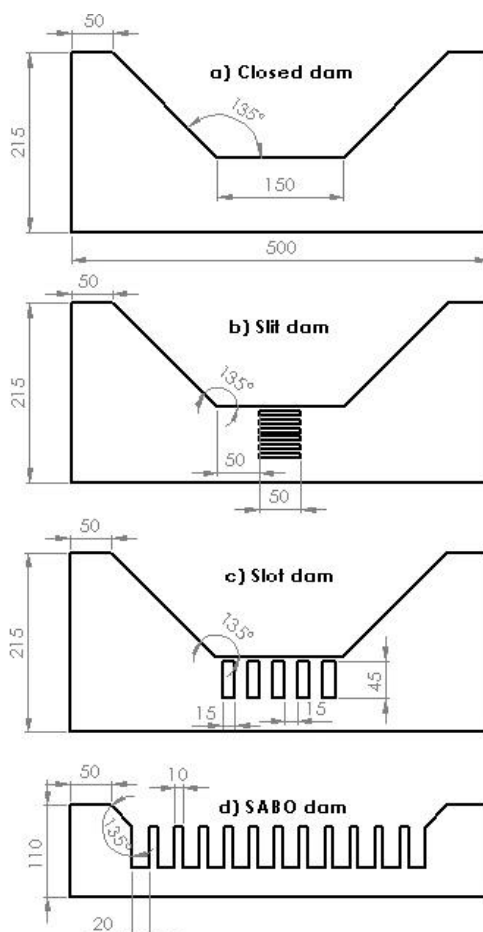
Figure 2. Dam tested a) closed dam, b) slit grilled dam, c) slot dam and d) SABO dam

3.3 LW mixtures

Five different mixtures of LW, called 1A, 1B, 2A, 2B, 3B, were prepared with fresh *Sorbus Aucuparia* stems of length 50 mm, 100 mm, 150 mm and eventually 200 mm (Table 1) and various diameters (Figure 3 and **Erreur ! Source du renvoi introuvable.**-3 in supplementary material). The wood density was measured in the range 0.745-0.83 with an average of 0.77.
160 Mixtures numbered "1" and "2" had maximum log length of 200 mm and 150 mm, respectively. Mixtures labelled "A" only consisted of coarse debris, i.e. logs, while mixtures labelled "B" also included fine material, here fresh pine tree needles. Mixture 3B was merely twice the mass of mixture 1B, i.e. contained roughly twofold greater number of elements, had a maximum log length of 200 mm and included fine material. Mixture 3B was prepared to test more intense LW supply. Overall, the solid volumes tested were high but not extreme. They would be equivalent for instance at scale 1:30 to 27-54 m^3
165 of solid volume in a reach 12 m wide, which would be 79-270 m^3 of LW jam assuming jam porosity (i.e., 1-solid volume/total jam volume) from 66 % to 80 % (Lange and Bezzola, 2006). Such amount of LW is sufficient to strongly disturb open check dam functioning to the experience of the authors.

Table 1. LW mixtures features

Mixture name	Number of logs by length (mm)				Fine material (pine needles)	Mean length (mm)	Mean diameter (mm)	Solid volume (10^{-3} m^3)
	50	100	150	200	FM	$L_{LW,mean}$	$D_{LW,mean}$	V_S
MIX 1A	114	88	31	**7**		87	7.8	1.04
MIX 1B	160	64	25	**5**	**Yes**	76	6.5	0.77
MIX 2A	279	11	16	-		67	6.2	0.94
MIX 2B	186	65	15	-	**Yes**	83	8.3	1.01
MIX 3B	332	131	65	**20**	**Yes**	82	7.4	**2.04**
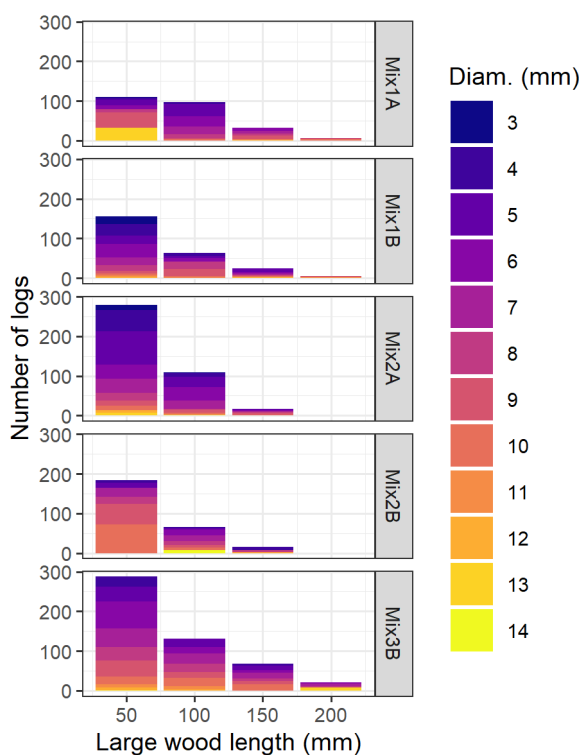
Figure 3. Number, length and diameter of coarse debris composing the LW mixtures

3.4 Experimental protocol

For each dam, two to three runs were performed in pure water conditions to check the repeatability and to calibrate the orifice and weir coefficients, μ_1 and μ_2, respectively. Three to four runs with each LW mixture were then performed to capture the random variation of LW jam formation, thus resulting in 15 to 20 independent runs with varying mixtures for

each dam. Each run consisted in a progressive increase in the discharge by 0.2 – 0.5 L/s steps from 0.5 L/s to full overtopping and release of all floating LW. The mixtures were progressively manually introduced in the flow from the first step. Acknowledging that LW recruitment and transfer is quite random in the field (Comiti et al., 2016), we did not try to define a relevant rate of LW introduction in the flume as done in other works (e.g., D'Agostino et al., 2000, Meninno et al.,

180   2019 or Rossi and Armanini 2019). An inverse approach was rather chosen trying to supply LW to make the jam "supply unlimited". We hypothesized that LW transported by the approaching or recirculating flows, i.e. LW of type (1) in Figure 1, generates marginal energy dissipation. Conversely, LW of type (2) and (3) in Figure 1, does not move, generates friction with flow and thus participates in energy dissipation. During experimental runs, it was made sure always to have LW of type (1) in the flume until LW mixture was entirely supplied. The LW jam could thus always grow up if flow conditions allowed

185   it. The protocol was thus to follow the rule "LW is to be added whenever all elements are stuck to the dam and no more element freely (re)circulates". This protocol has the advantage of avoiding mechanisms related to specific LW recruitments and transfer scenarios and is expected to prevent eventual side effects of arbitrary choice on LW supply rate.

The experimental data comprises 649 flow depth and discharge measurements of which one quarter concerns pure water experiments and three quarters concern LW (data provided in appendix of Piton et al., 2019b). The head loss Δh was

190   computed as the difference between h, the depth measured with LW, and h_0, the depth computed in pure water condition, i.e., using Equation 4 with the same discharge and setting $\beta_1 = \beta_2 = 0$. The β_i coefficients were then computed in several steps (Figure 4): (i) β_1 was computed using Equation (2) for each measurement where no or slight overflowing discharge was observed, (ii) bounds of β_1 were determined out of all these measurements, (iii) β_2 was computed using Equation (4) for all measurements considering β_1-bounds and their average and (iv) bounds of β_2 were computed on discharges strongly

195   overflowing. Since β_1-bounds are calibrated for no and low overflowing while β_2-bounds are calibrated on high overflowing, points transparency on the following figures are increased where they lose relevance.
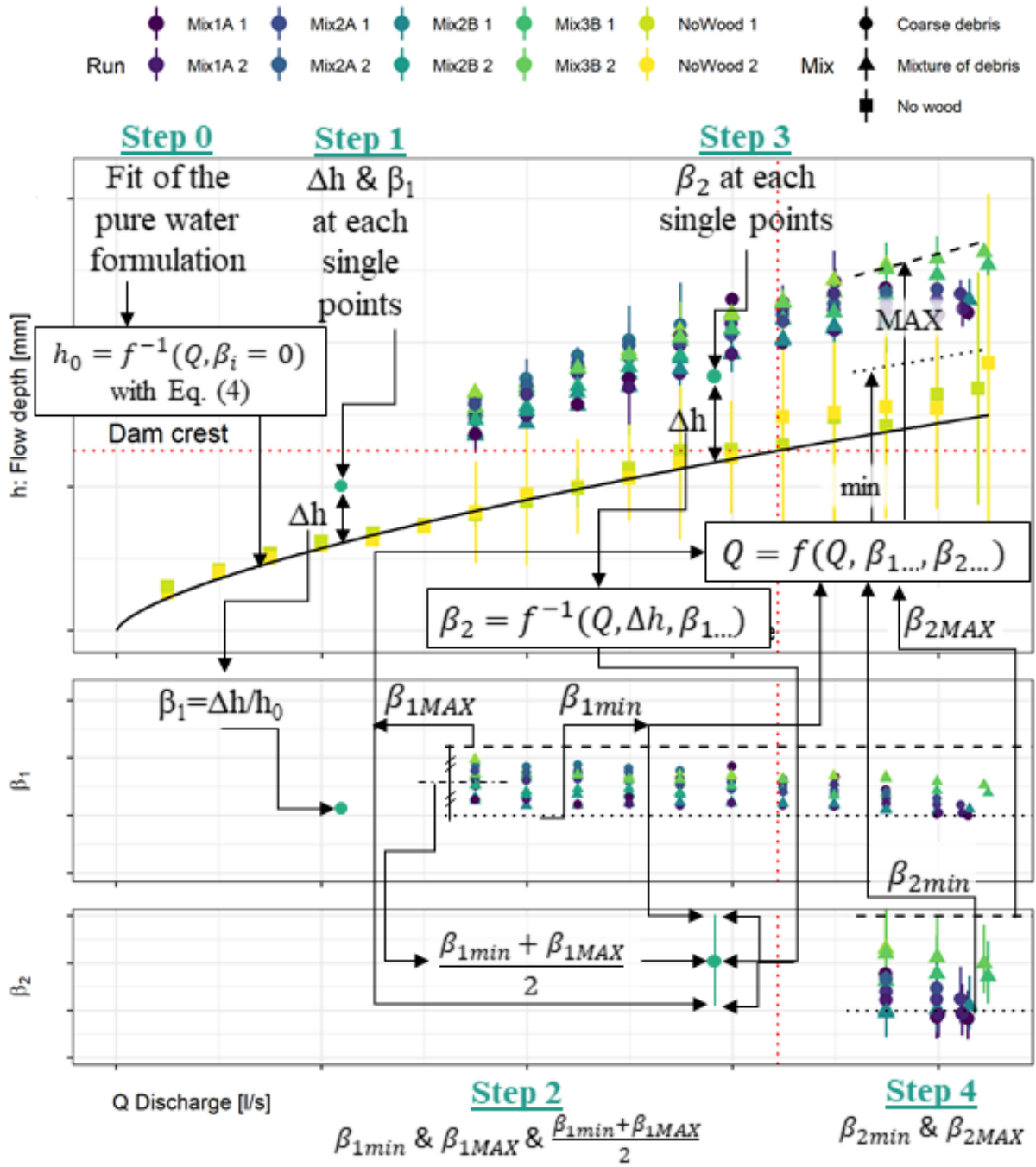
Figure 4. Computation steps for β_1 and β_2

4 Results

Results are organized in three sections: (i) a qualitative description of the interaction between LW and barriers, (ii) quantitative analysis of head losses in each dam and (iii) release conditions for all dams.

4.1 Main phases of LW jamming and releases

The same main phases of the process were observed during most runs with LW (Figure 5).

4.1.1 Phase 1: accumulation against the dam

During phase 1, LW approached the openings and a few pieces eventually passed through the dam (Figure 5a-b). LW elements were mostly stuck against the dam, approaching generally floating in a horizontal position. They get stuck against and often parallel to the dam. At each discharge step, flow depth increased progressively up to a new stable value. LW reorganized at each flow depth change generating increasing obstruction of the openings. LW stuck against the openings seldom moved upward with the free surface level change but rather stayed stuck at their position due to the drag force, the friction with opening borders and eventual entanglement in the openings and in the LW jamming. Neighbouring elements could thus approach the dam and openings for any sufficient water depth increase. They were consequently piling up over other jamming LW pieces and progressively obstructed all the upstream face of the dam. LW elements not stuck against the dam were either (see figure 1): (1) Floating freely and moving with flows, (2) Organized close to the dam in a quasi-immobile "floating carpet", or (3) Dragged underneath the carpet, after impact on the floating LW, and reached the openings or get stuck against other logs. The latter required that flow through openings was significant and was consequently mostly observed with the SABO dam, as well as with the slot dam though in a lesser extent. Phase 1 was not observed on the closed dam since it had no openings.

4.1.2 Phase 2: overflowing with possible LW release

Phase 2 started when overflowing on spillway reached a sufficient depth to (eventually) release some LW, i.e., when flow depth approached or passed the LW diameter. The floating carpet followed the free surface level and was then in a position higher than the dam crest. The floating carpet arrangement was modified regularly - notably at increases of water depth - because of impact of LW upstream or following the release of a few LW pieces finding a way over the spillway (compare e.g., Figure 5c-d and e-f). The floating carpet was in a position theoretically prone to be released during this phase but was usually not, due to the spillway obstruction by LW elements (i) arching the spillway, (ii) entangled in the openings or (iii) entangled in other submerged stable logs. In dams with small openings, i.e., the slit and slot dams, floating carpets could be quite extensive while lateral views demonstrated that the openings were jammed only by a few pieces (e.g., Figure 5c-d). The SABO dam had such a large proportion of the flow that could pass through the dam that even when overflowed, newly supplied-LW were again regularly dragged underwater and fed the submerged jam.

Lower discharge passing through the dam induced lower number of LW to be submerged and more developed
230   floating carpet. The LW elements obstructing the spillway were sometimes very stable, typically when arches formed or if
one element took vertical position, protruded above water surface thus behaving as a pole and offering a new point to form
stable arches.

4.1.3   Phase 3: actual LW release

Nonetheless, Phase 3 consisting in sudden and massive releases of all floating LW was systematically observed on
235   the closed, slit and slot dams. Phase 3 was observed on the SABO dam only three times due to experimental limitation: the
maximal discharge capacity of 8.9 L/s was only approaching the conditions for sudden releases. Releases occurred for higher
discharges on the SABO dam because (i) the ratios between water depth and dam height were small due to the high
permeability, thus limiting the overflowing discharge and (ii) the 11 openings enabled numerous pieces to be entangled and
to protrude over the dam crest, thus creating numerous obstacles to the release of the floating elements. Phase 3 would be
240   observed on the SABO dam on all runs for sufficiently high discharge without any doubt.
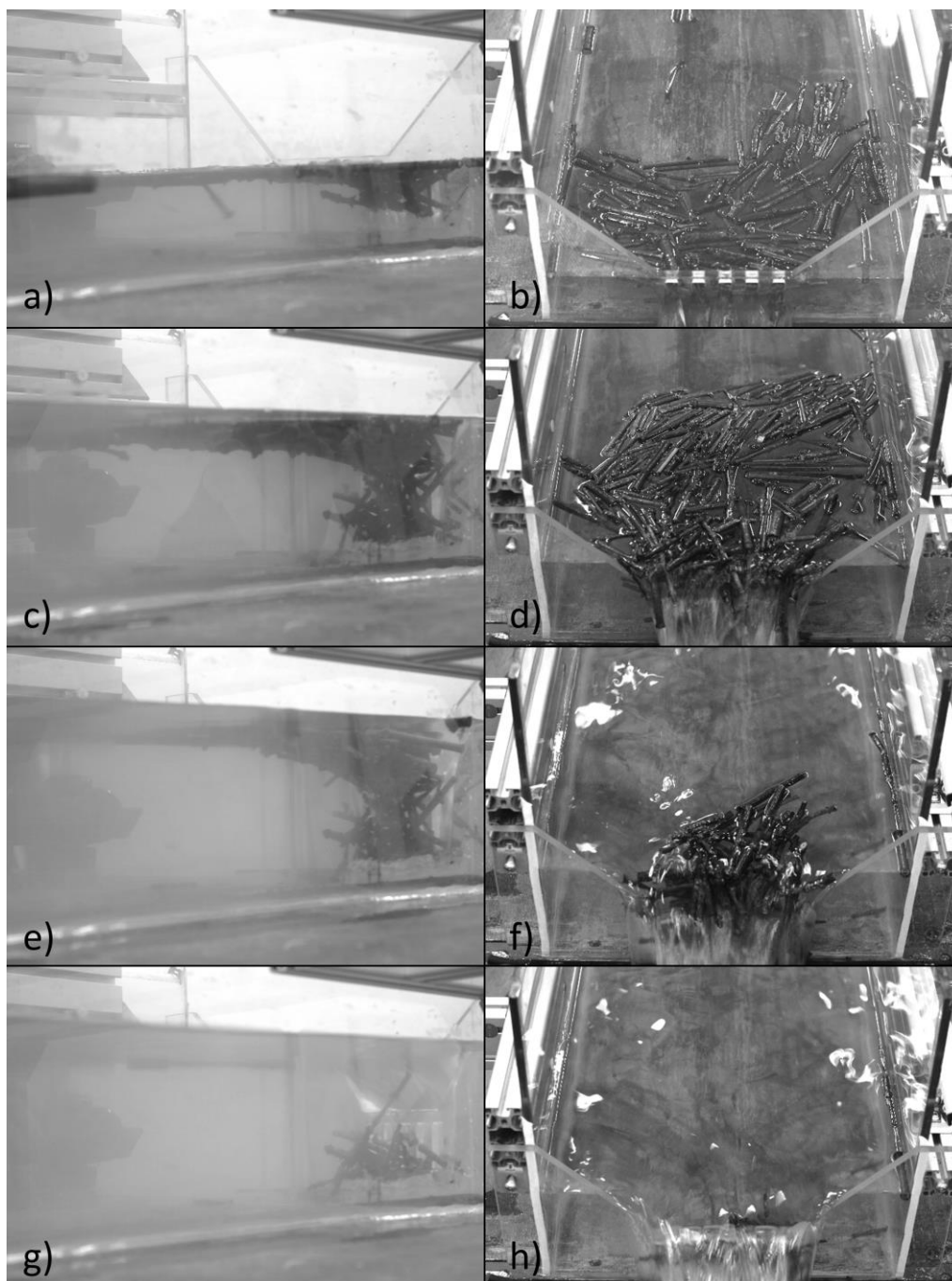
Figure 5 : Example of phases observed during most runs (illustrated here with Mix A2, repetition #2 on slot dam) : Phase 1 – LW simply stuck against the dam, a few floating LW apart, here at discharge 0.5 L/s, (a) side view and (b) top view ; Phase 2 – slots jammed and floating carpet developed upstream, here at discharge 3.5 L/s, (c) side view and (d) top view ; Phase 2 later – denser jam for higher discharge (here at 5.4 L/s), several pieces yet released, (d) side view and (e) top view and, 5 second later the LW overtopped the barrier and Phase 3 – final state after jam overtopping occurs here still for discharge 5.4 L/s, (g) side view and (h) top view

4.2 LW-related head losses and stage –discharge relationships

The first objective of this paper is to provide a way to compute the increase in water depth eventually observed upstream of check dams in presence of LW. The calibration of dimensionless coefficients of weir and orifice as well as coefficients β_1 and β_2 are provided in the next sections for each dam tested. Their intercomparison is later provided in the discussion.

4.2.1 Closed dam

The weir coefficient was calibrated at $\mu_2=0.4$ based on the pure water runs (Figure 6). This value was later re-used in Eq. (4) for all other dams. The value was calibrated on discharges higher than 1 L/s such that overtopping depth was higher than 1.5 dam thickness and the narrow-crested weir hypothesis holds. Using Eq. (3) with $\beta_2 = 0.05$ and $\beta_2 = 0.4$, provide satisfying lower and upper bounds, respectively, of the 98 points measured with LW on the closed dam (Figure 6). Coefficient β_2 was directly computed without approximation for this dam since determining β_1 coefficient is not relevant due to the absence of opening. A slight but not systematic decreasing trend in β_2 can be observed when discharge increased which is related to the LW accumulation rearranging as discharge increased. LW releases occurred mostly for discharge between 1.5 and 2.5 L/s, thus the few points for Q > 2.0 L/s.
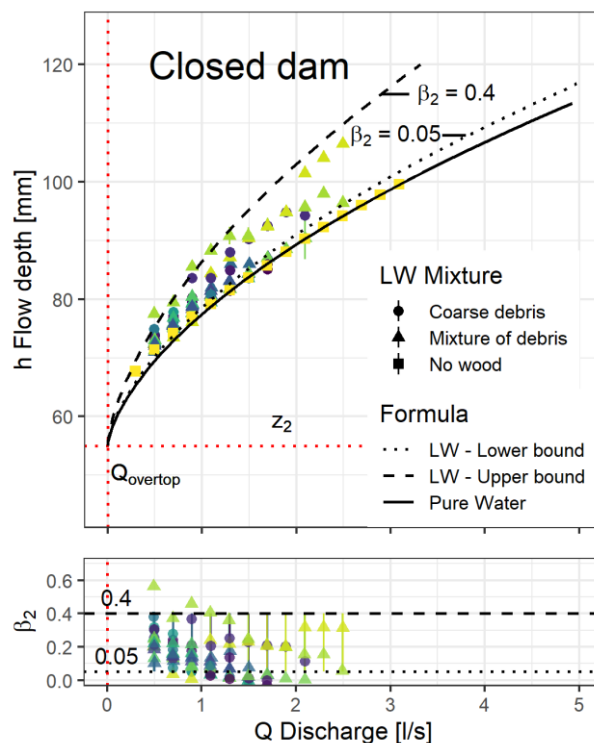
Figure 6. Flow depth versus discharge for closed dam and back-calculated β_2 values, each color shade corresponds to a different run

4.2.2 Slit dam

The orifice coefficient of the slit dam was calibrated at $\mu_1 = 0.42$, namely 65 % of 0.65, which is the value proposed
265 for a single slit without grill by Piton et al. (2016). This result is consistent with the 50 % obstruction of the slit by the grill
and the correction coefficient provided by Piton and Recking (2016a) for grilled slits. Using Equation (4) with $\beta_1 = 0.05$ and
$\beta_2 = 0.2$ or $\beta_1 = 0.25$ and $\beta_2 = 0.6$, provides satisfying lower and upper bounds, respectively, of the 85 points measured with
LW on the slit dam (Figure 7). A few points related to one single run reached β_2 values slitghly higher. Both coefficient β_1
and β_2 show slight decreases with increasing discharge and are often maximum close to the transition between phase 1 and
270 phase 2, i.e., when flow starts really to overtop the dam.
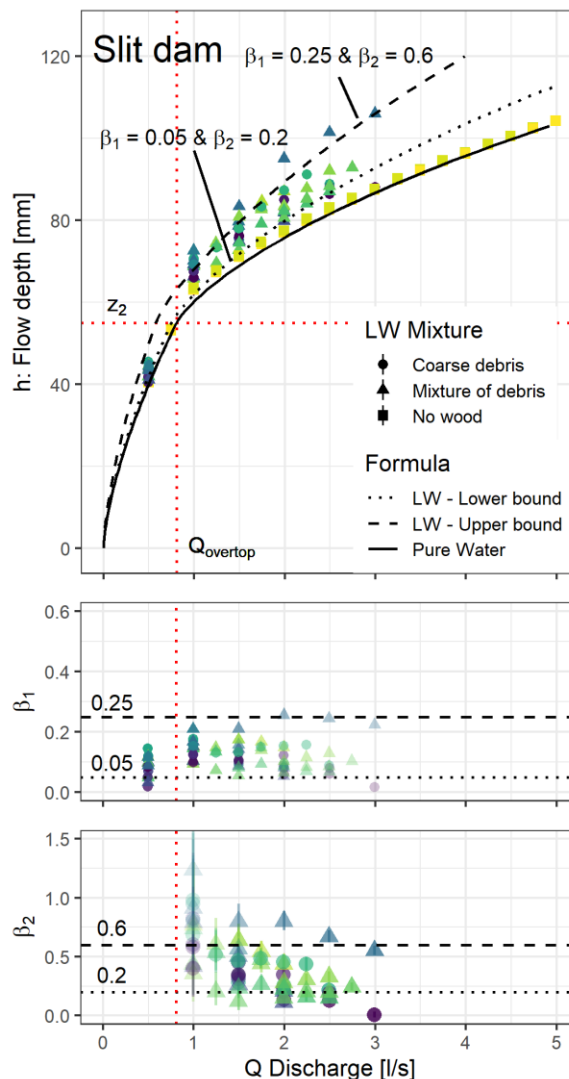
Figure 7. Flow depth versus discharge for grilled-slit dam and back-calculated β_1 and β_2 values, each color shade corresponds to a different run

4.2.3   Slot dam

275   The orifice coefficient of the slot dam was calibrated at $\mu_1 = 0.72$, i.e., 110% of the standard value of 0.65 proposed for a single slit. This is likely related to the influence of several orifices close from each other. They enable current lines to be more smoothly arranged preventing sharp angle for the current lines of the central slots (see also SABO dam below). Using Equation (4) with $\beta_1 = 0.15$ and $\beta_2 = 0.2$ or $\beta_1 = 0.6$ and $\beta_2 = 0.6$, provides satisfying lower and upper bounds, respectively, of the 127 points measured with LW on the slot dam (Figure 8). Both coefficient β_1 and β_2 show again slight

280   decreases with increasing discharge and are again maximum close to the transition between phase 1 and 2, i.e., when flow starts overtopping the dam. It is interesting to note that the lower and upper values of β_2 are similar for the slit and the slot dams.
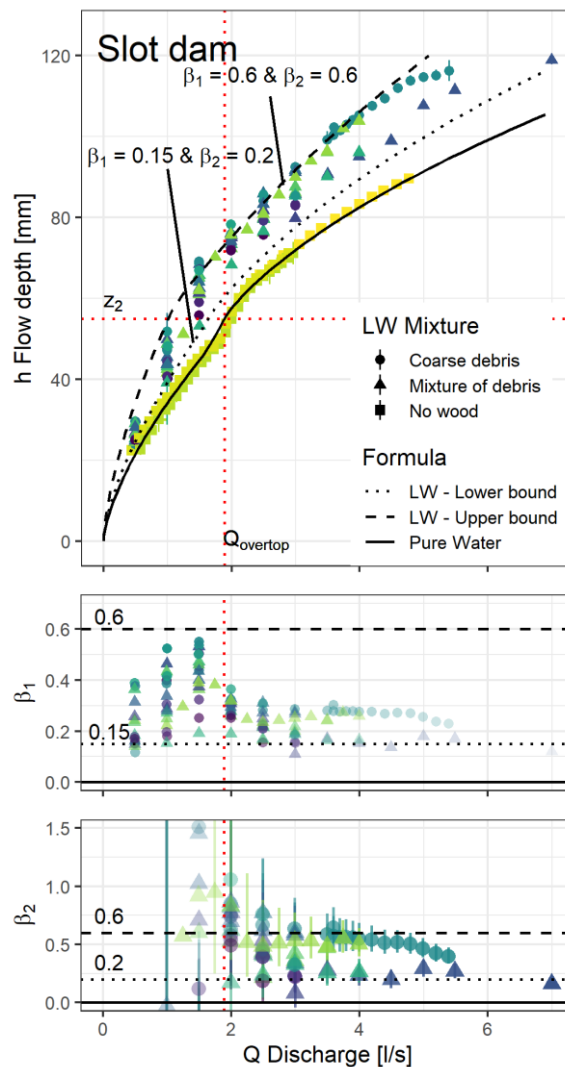
Figure 8. Flow depth versus discharge for slot dam and back-calculated β_1 and β_2 values, each color shade corresponds to a different run

4.2.4   SABO dam

The orifice coefficient of the SABO dam was calibrated at $\mu_1 = 0.81$, i.e., 125 % of the standard value of 0.65 for one single slit. With 11 openings, i.e., 6 more opening parts than the slot dam, the stream lines are likely even better arranged which probably explains this better hydraulic capacity. Some experimental arrangement at the flume inlet were necessary to enable pushing the pump capacity to its maximum but waves appeared in the flume and disturbed greatly the free surface level measurement. The visible high error bars for some runs and especially the pure water ones are an artefact of these waves and the deviation from the theoretical curve for $Q > 5.0$ L/s should not be considered relevant. This problem was fixed on most measurements with LW with beneficial effect on the error bars. Using Equation (4) with $\beta_1 = 0.5$ and $\beta_2 = 0.5$ or $\beta_1 = 1.1$ and $\beta_2 = 2$, provides, respectively, satisfying lower and upper bounds of the 186 points measured with LW on the slot dam (Figure 9). Both coefficients β_1 and β_2 show here again slight decreases with increasing discharge and are again maximum close to the transition between phase 1 and 2, i.e. when flow starts overtopping the dam which occur much later than for the other dams.
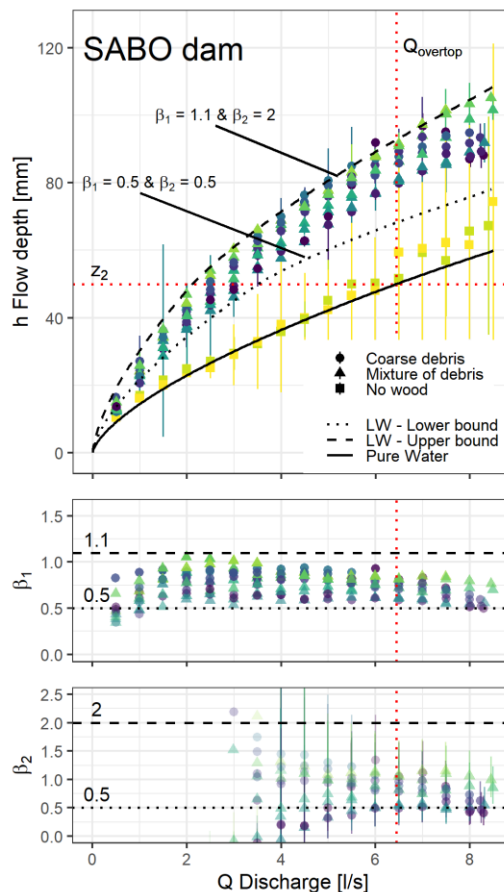
Figure 9. Flow depth versus discharge for SABO dam and back-calculated β_1 and β_2 values, each color shade corresponds to a different run

4.3 Release conditions

300

The second objective of this paper was to describe conditions leading to release of LW downstream by dam overtopping. In order to transfer the results of this study, some dimensionless numbers were defined to characterize the flow conditions and eventually the domain where LW releases were observed, i.e., where trapping efficacy drops suddenly. Furlan (2019) identified that the probability of logs to be trapped by reservoir dam spillways was first related to the ratio

305 between overtopping depth and log diameter. The dimensionless overtopping depth h^* (-) is consequently defined by:

$$h^* = \frac{h - z_2}{D_{LW,mean}} \qquad (5)$$

Where, $D_{LW,mean.}$ is the mean log diameter of the LW mixture (m). Furlan (2019) also studied the effect of log density that was ignored in this study.

Figure 10 displays the percentage of LW released against h^*. It can be observed that most "significant" releases, i.e.

310 >10%, occurred in the range $3.0 < h^* < 5.0$. A few releases were also observed for much higher overtopping, up to $h^* = 10$. They occurred for LW jams stabilized by logs arching the weir or by logs tightly entangled in the submerged elements. The LW max length might play a marginal role for the closed dam and for the SABO dam where releases occurred more for mixtures with a smaller max length but this was not consistently observed for all dams. Log max lengths being either 150 mm or 200 mm and weir base width being at least 150 mm wide, conditions with very high probability of stable arching

315 of weir (Piton and Recking, 2016b), i.e., with log length longer than twice weir width were not tested. Consequently, log length was a marginal effect on release condition.
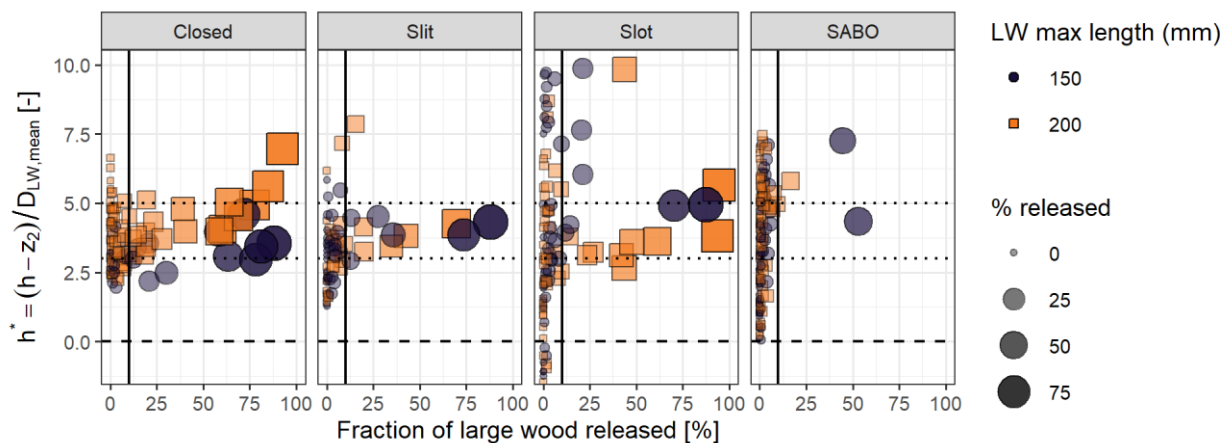
Figure 10. Percentage of LW released (i.e. mass fraction of LW released during one discharge step over total sample mass) against dimensionless overtopping depth, dot size and opacity proportional to LW released. The continuous vertical line marked the 10% released

320 that was fixed arbitrarily as the threshold value for significant LW release

The dimensionless overtopping depth h^* was not sufficient to capture the overtopping process. In essence, floating carpets (type 2 in Figure 1) were observed to be more easily released than LW submerged in number and tightly entangled (type 3 in Figure 1). Jams against the SABO dam were for instance rarely released even for $h^* > 5$. The balance between

buoyancy and drag force governs the shift from the regime of floating carpet to the regime of submerged jam. In the line of
Kimura and Kitazono (2019), a dimensionless number figuring whether buoyancy or drag force dominated is hereafter
defined to discriminate which kind of jam might form. Buoyancy, noted Π hereafter, was computed considering the logs
nearly to be submerged i.e. with their full volume under water surface:

$$\Pi = \frac{g(\rho-\rho_s)\pi D_{LW\,mean}^2 L_{LW\,mean}}{4} \tag{7}$$

With ρ and ρ_s the water and LW density, respectively (kg/m³). The drag force F_D was computed using:

$$F_D = \frac{1}{2}\rho C_D D_{LW\,mean} L_{LW\,mean} u^2 \tag{8}$$

With C_D the drag coefficient (-) taken equal to 1.2 for logs without branches (Merten et al., 2010; Ruiz-Villanueva et al.,
2014a), and u is the flow velocity near the log (m/s). This formulation relies on several hypotheses: (i) the log is considered
in a transverse position with respect to flow direction and quasi-submerged, consistently with the hypothesis made for
buoyancy, thus the surface of the log being proportional to its diameter times its length, (ii) the log is quasi-immobile so the
full velocity of the flow is considered, (iii) the precise value of u in the direct vicinity of the logs is unknown but the cross
sectional averaged velocity is considered relevant as a first approximation thus $u \approx V = Q/(hW)$ with W the flume width (here
0.4 m). We define the dimensionless number called buoyancy to drag force ratio Π/F_D as the ratio between Eq. (7) and Eq.
(8) that can be rearranged as follow:

$$\frac{\Pi}{F_D} = \frac{\pi}{2C_D}\frac{\rho-\rho_s}{\rho}D_{LW\,mean}\frac{gW_{mean}^2h^2}{Q^2} = \frac{\pi}{2C_D}\frac{\rho-\rho_s}{\rho}\frac{D_{LW\,mean}}{h}\frac{1}{Fr^2} \tag{9}$$

Theoretically, a log in a context where $\Pi/F_D \gg 1$ should float since buoyancy prevails, that should be the "floating
carpet domain". Conversely, a log can be submerged, sucked and dragged by the flow below the water surface in a context
where $\Pi/F_D \ll 1.0$, which should be the "piling jam domain".

Figure 11 displays Π/F_D versus $h*$ with the size of dots proportional to the amount of LW released. In addition, a smoothed
trend related only to points with released LW fraction higher than 10% was computed using the stat smooth function, loess
method of the ggplot2 library in R (Wickham, 2016) and plotted in orange. This statistical fit overall confirms that most
releases appeared for $3.0 < h* < 5.0$, although it highlights particular behaviour for high and low values of Π/F_D. In the floating
carpet domain, i.e., when $\Pi/F_D \gg 1$, the threshold value for overtopping of $h*$ is comprised in the range 3-5, slightly
decreasing for $\Pi/F_D > 3.0$ and approaching the critical values of $h*=1.5-2.0$ identified by Furlan (2019) for dam reservoir
spillway.

In the piling jam domain, i.e. when $\Pi/F_D \ll 1.0$, the few available observations suggest a significant increase in flow
overtopping, $h*$ with decreasing Π/F_D. This is due to drag force being higher than buoyancy force, favouring piling up,
dense 3D jams and strong friction between logs. Close from the threshold, i.e. for $\Pi/F_D \approx 1.0$, the range 3.0-5.0 is still
applicable. As said before, a few points, related to randomly-generated very stable arrangements may reach higher values of
$h*$, e.g. the few black squares with $h* \approx 6.0-7.0$ related to jams retained by arching logs across the weir. Small transparent
points appear for $h* < 0$ and are related to a few logs passing through the dams' openings.
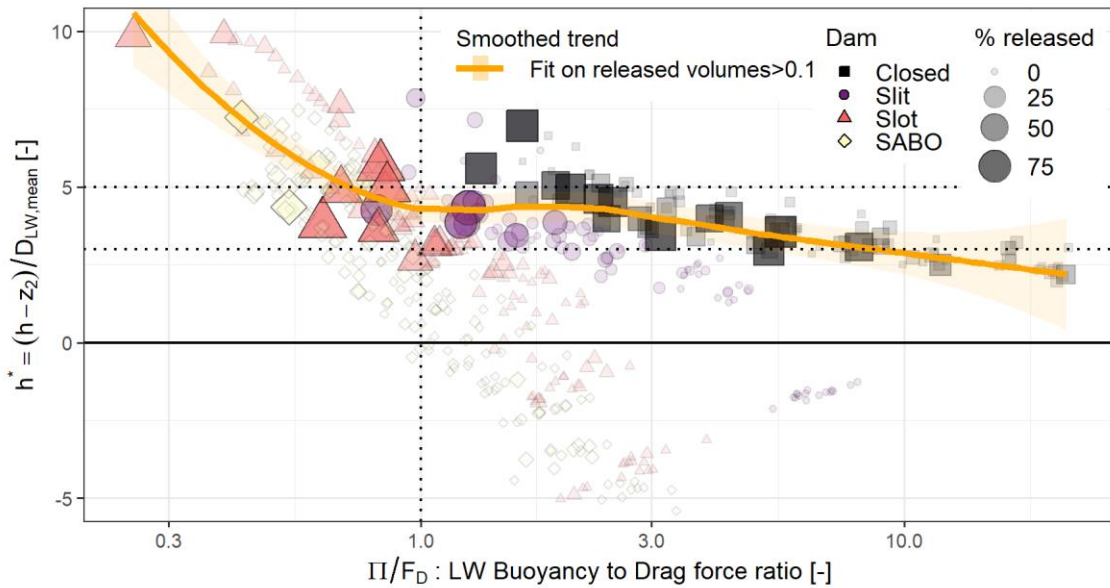
Figure 11: Dimensionless overtopping depth h^* VS buoyancy to drag force ratio Π/F_D with dot size and opacity proportional to the amount of LW released. Releases occur for lower h^* in the $\Pi/F_D \gg 1.0$, i.e., if buoyancy prevails and floating carpets forms while releases occur for higher h^* if dense jams forms under high drag forces in the $\Pi/F_D \ll 1.0$ domain

5   Discussion

5.1   Comparison with existing studies

Past works on interactions between LW and dams studied LW-related head losses or trapping efficacy, i.e., somewhat the opposite of release conditions (Table 2). No works so far addressed in such details compound structures with both openings and an upper spillway as the present paper. The results of the experiments presented in this paper are also included in Table 2 using $\Delta h/h_0$, which encapsulates the balance between Q_1 and Q_2 and thus effects of both β_1 and β_2. Values of $\Delta h/h_0$ measured in past works in quite different structures than the one tested in this paper are very consistent:

(i) overflowing structures as dam spillway, PK-weirs and our closed dam experience the smallest $\Delta h/h_0$ values ranging in 0-50%;

(ii) slit and slot dams experience slightly higher $\Delta h/h_0$ ranging in 5.0 %-60 % with lower values when grills protect the slit; and

(iii) widely open structures as SABO dam and racks experience high values of $\Delta h/h_0$ ranging in 20 %-100 % , for subcritical incoming flows (up to 210 % as in the experiments of Schmocker and Hager, 2013, who used high LW volumes), and ranging in 170 %-230 % for supercritical incoming flows (up to 330 % for high volume of LW - Schmocker and Hager, 2013).

375 Supercritical conditions results in very high $\Delta h/h_0$ because h_0 are low, while their relative energy loss $\Delta H/H_0$ are of the same order of magnitude than for subcritical flows (see appendix for detailed computation of $\Delta H/H_0$). $\Delta H/H_0$ are typically up to 0.6-0.7 for average LW volumes and up to $\Delta H/H_0 \approx 1.5$ for high volume of LW. Using relative energy loss $\Delta H/H_0$ rather than relative head loss $\Delta h/h_0$ in future work is recommended since it removes the bias related to the lack of kinetic energy in the ratio $\Delta h/h_0$. Indeed a key part of kinetic energy transforms in height when strongly supercritical flows reach subcritical flows

380 in the vicinity of hydraulic structures jammed by LW.

Table 2: Literature review of existing results on LW-related head losses and release conditions

Type of structure	Ranges of $\Delta h/h_0$ ($\Delta H/H_0$)* [Fr_0]**	Volume of LW	Parameter driving LW downstream releases	Comment	Reference	Work main topic***
Reservoir dam spillway	0.05-0.5 [0,05 ; 0.35]	Mean		Test begun with $h \gg D_{LW}$	(Hartlieb, 2012, 2017)	HL
-	0-0.3 [0,01]	Very small	$h/D_{LW} > 1.5$ $W_0/L_{LW} > 0.8$		(Furlan, 2019)	TE
Piano-key weir	(0-0.2) Unknown Fr_0	Very small	$h/D_{LW} > 3$ ($h/D_{LW} > 10$ with branches and root wads)	$\Delta H/H_0$ up to 0.6 for low discharge	(Pfister et al., 2013a, 2013b)	HL
Closed check dam	0.05-0.4 [0.01-0.1]	Mean	$5.0 > h/D_{LW} > 3.0$		This paper	HL & TE
Slit dam with inclined grill	0-0.1 [0.07]	Very small	Unknown	No overtopping	(Meninno et al., 2019)	HL & TE
Slit dam with grill	0.05-0.3 [0.05-0.1]	Mean	$5.0 > h/D_{LW} > 3.0$		This paper	HL & TE
Slit dam	0.05-0.6 [0.07]	Very small	$W_0/L_{LW} > 1/2$ (for small LW discharge : 8-14 logs/s)	No overtopping	(Meninno et al., 2019)	HL & TE
-	-	-	$W_0/L_{LW} > \approx 1.0$ (for high LW discharge : 150 logs/s)	-	-	HL & TE
Slit dam	Unknown head losses and Fr_0	Medium to high	$W_0/L_{LW} > 1$	No overtopping, debris flow experiments	(Chen et al., 2020)	TE
Slot dam	0.05-0.6 [0.1-0.15]	Mean	$6.0 > h/D_{LW} > 3.0$		This paper	HL & TE
SABO dam	0.2-1 (0.2-1) [0.4-0.5]	Mean	$7.0 > h/D_{LW} > 4.0$		This paper	HL & TE
SABO dam	0-1.2 [2.5-2.8]	Low	$W_0/L_{LW} > 0.5-0.75$		(Horiguchi et al., 2015)	TE
Rack made of piles	1.0-2.1 (0.8-1.4) [0,5 ;0.8]	Very high	Marginal releases (2.0 %-8.0 %)	No overtopping,	(Schmocker and Hager, 2013)	HL
-	3.0-3.3 (0.9-1.1) [1.5]	-	-	-	-	HL
-	0.3-1 (0.2-0.7) [0,3 ; 0.75]	High	Marginal releases (0%-5.0 %)	No overtopping	(Schalko et al., 2019a)	HL
-	1.7-2.2 (0.5-0.6) [1.2 ; 1.6]	-	-	-	-	HL

*Ranges of $\Delta H/H_0$ are not provided when upstream Froude number Fr<0.3 because $\Delta H/H_0 \approx \Delta h/h_0$
** Range of Fr in pure water condition
*** HL: Head Losses; TE: Trapping Efficacy

5.2 First step toward generalization

Four types of dam were tested in this paper. In order to transfer the results to other open check dam configurations, dam permeability was computed using Void Ratio (Di Stefano and Ferro, 2013), namely the cumulated opening width normalized by the flume width W (m):

$$\text{Void ratio} = \frac{\sum_N w_1}{W} \qquad (10)$$

Dams with higher permeability have higher void ratio and also higher discharge passing through and thus flow power to stuck LW against the dam, thus increasing β_1 (Figure 12a). Meanwhile β_2 increase too because the dense jam created against the dam piles up and obstructs the barrier crest as well (Figure 12b). Consistently, the lower the permeability and thus the void ratio, the bigger the initial water depth for a given discharge. A corollary is that higher water depth means slower flow and higher likelihood to stay in the floating carpet regime, thus preventing piling up of LW against the dam and higher β_1 and β_2. Void Ratio is obviously correlated with Π/F_D: high Void Ratio reduces h and thus Π/F_D (see Eq. 9). However, we do not provide a graph showing β_i against Π/F_D because water depth h is involved in the computation of both variables, thus generating spurious correlation in such a graph; a drawback that the Void Ratio does not have.
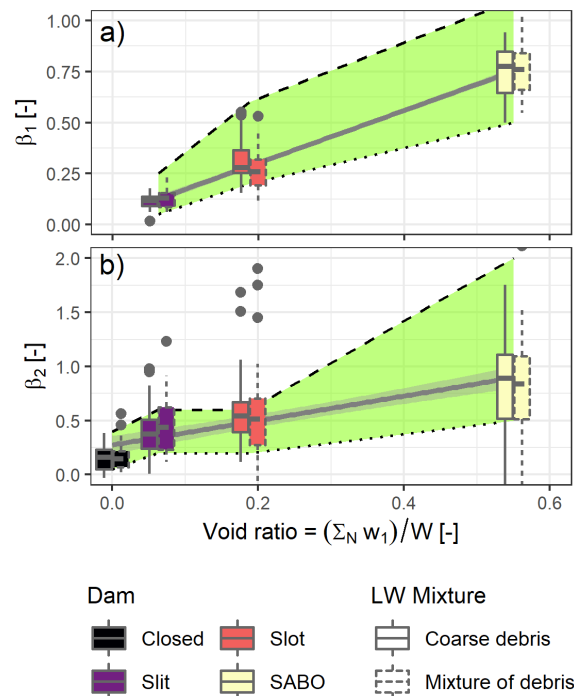
Figure 12. *Variability of β_1 and β_2 versus void ratio for all dams. Boxes display first, second and third quartiles, points are outliers higher than the 1.5 the interquartile range. Grey lines are linear fits on all data highlighting the increasing trends. The light grey ribbon and dotted lines show the upper and lower bounds fitted for each dam. Overall headloss coefficients increase with barrier permeability but presence of fine material or only of coarse debris has marginal influence*

Using the results of this paper, it seems possible to bound the possible effect of LW reaching an open check dam. Only a bounding is possible because random variations in the arrangement and effects of LW are incompressible. In a first step, the range of flow depth h possibly observed for a given discharge can be computed with Eq. (4) and the lower and upper bounds

405 of β_1 and β_2 for the selected type of dam (using values from Table 2 or eventually an interpolation in Figure 12 with the Void Ratio). Assuming a range of h, it is possible to compute ranges of h^* and Π/F_D with Eqs. (5) and (9). If the flow is systematically in the floating carpet domain, LW releases are likely to occur either (i) in the range $3 < h^* < 5$ if $1 < \Pi/FD < 10$ or (ii) in the range $1.5 < h^* < 3$ if $\Pi/F_D > 10$. If conversely flows enter the piling jam domain, i.e. where $\Pi/F_D < 1.0$, it can be expected that LW releases occur for $h^* > 3$, up to $h^* \approx 10$ for $\Pi/F_D \approx 0.3$. When structures width are close to

410 LW length or equipped with openings, it cannot be excluded that LW forms arches or get entangled in openings and in the LW jam, thus resulting in h^* triggering releases, the narrower the structure and the more numerous the opening, the higher the h^* increase. It is known that for log length two to three time longer than opening width, the trapping efficacy become very high and release become unlikely (Piton and Recking, 2016b).

5.3 Other application of Π/F_D: Back analysis of numerical 1D and 2D models

415 Another possible use of our approach could be to identify where floating carpets or dense 3D jams might form using results of numerical models based on shallow water equations (thus, computing depth-averaged velocities). Diverse approaches to compute LW trajectories and effects were proposed (Addy and Wilkinson, 2019; Stockstill et al., 2009). The advanced way fully describing log trajectories by coupling depth-averaged models with Lagrangian descriptions of logs currently relies on the hypothesis that logs are floating (Ruiz-Villanueva et al., 2014a), i.e., on the hypothesis that flows stays

420 in the floating carpet domain. It would be easy to create maps of Π/F_D based on numerical model results, which could help to identify where flows leave the floating carpet domain, i.e. areas where the model might underestimate LW jam packing and where the result interpretation should be consider with more caution. Using 3D flow models makes possible to compute more in detail LW behaviour but requires much more computational power (Kimura and Kitazono, 2019).

5.4 Limitations of the approach

425 #### 5.4.1 Non-unique constant head losses coefficient

Trends of increases followed by decreases of β_i with discharge were highlighted in Figure 6-9 and could be modelled with a statistical approach. The scattering related to the random variation between runs is, however, bigger than the variation with discharge for a given run. The approach proposed by this paper aiming at being simple to use, constant values of β_i were retained rather than β_i coefficients changing with Q or Π/F_D.

430 When the dam crest is overflowed, discharge $Q = Q_1 + Q_2$ and the head loss Δh is the fruit of both β_1 and β_2. For a given couple $(h = \Delta h + h, Q)$, several couples of values of β_1, β_2 may be considered (Figure 4). There is thus a non-uniqueness of possible β_i parameters for each couple. We overcome this non-uniqueness by defining constant β_i parameters bounding the

whole range of discharge for each dam. A sensitivity analysis using other β_i coefficients is provided in supplemental material to demonstrate that using lower or higher values of β_1 or β_2 does not allow describing each entire sample.

435 **5.4.2   Uncertain buoyancy to drag force ratio**

It is worth being stressed that the way buoyancy, drag force and thus Π/F_D are computed relies on several crude hypotheses presented above. Π/F_D is clearly not an accurate ratio capturing all the subtle effects of log shape, roughness and flow approaching conditions. Π/F_D also ignores the effect of other logs, antecedent flow conditions or the complex flow 3D pattern in the dam and jam vicinity. Π/F_D should merely be considered a proxy of the buoyancy to drag force ratio to identify

440 in a coarse way whether LW might accumulate as a floating carpet or as in a dense 3D jam. Further experiments aiming at refining the threshold value of Π/F_D and its uncertainty are necessary. Other formulations, using more detailed expressions of drag force or buoyancy or other dimensionlesss numbers, could be relevant. Kimura and Kitazono (2019) for instance proposed to use the driftwood Richardson number DRI=$(\rho_s$-$\rho)/(\rho Fr^2)$, which is the ratio between buoyancy and inertial force, to discriminate LW accumulating against bridge piles as floating carpet or in 3D jams. Π/F_D worked better than DRI on our

445 data so we did not push further their concept but they inspired us to define Π/F_D.

6   Conclusion

Debris basins equipped with open check dams are key structures in the mitigation of hazards due to solid transport (sediment and LW). Open check dams aim at trapping all or part of sediment and/or LW. They are compound structures with opening part through the dam and safety spillway atop. These hydraulic structures are usually designed considering, on the

450 one hand, transported element sizes and opening sizes to assess the clogging probability and, hydraulic equations to estimate flow depth, overflowing height and basin filling. Although LW proved to profoundly trouble open check dam functioning in the past, its accumulation is still often ignored in the design, notably due to the lack of comprehensive study on LW effects on open check dam hydraulics. In the worst cases, open check dams are overflowed by such a depth that LW are finally suddenly released, eventually triggering high damage aggravation downstream. The few works addressing LW releases were

455 so far only dedicated to reservoir dam spillways.

This paper presents a comprehensive analysis of the disturbance induced by LW in open check dam hydraulics and of their release conditions. A framework of analysis using simple dimensionless coefficients was developed to compute the relative increase in water depth related to LW presence. We demonstrated that flow depth might increase by 5%-40% on weir, 20%-60% on slit and slot dams and 50% - 200% on racks and SABO dams. These results are consistent with data from literature

460 on dam reservoir spillways or on LW racks, and thus seem transferable to other similar structures.

In addition, it was highlighted that LW may be released over the structures for overflowing water depth higher than 3-5 LW-diameters. This value is higher than the range $1.5 - 2$ LW-diameters measured on dam reservoir spillways because LW tends to entangled more tightly against open check dams than in the tranquil lakes formed by reservoir dams. In order to anticipate

whether the LW might accumulated as a single-layer floating carpet or as a dense 3D jam, a new dimensionless number was
465   proposed. This ratio of buoyancy to drag force captures, without calibration, the transition from the regime of floating
carpets to the regime of dense multi-layer jams, the latter being more stable, released for higher flow depths but also trigger
higher head losses.

Appendix A

Relative energy loss is computed using:

470   $$\frac{\Delta H}{H_0} = \frac{H-H_0}{H_0} = \frac{H}{H_0} - 1 = \frac{h\left(1+\frac{Q^2}{2gh^3W^2}\right)}{h_0\left(1+\frac{Q^2}{2gh_0^3W^2}\right)} - 1 = \frac{(h_0+\Delta h)\left(1+\frac{Q^2}{2gW^2(h_0+\Delta h)^3}\right)}{h_0\left(1+\frac{Fr_0^2}{2}\right)} - 1 =$$

$$\frac{\left(1+\frac{\Delta h}{h_0}\right)\left(1+\frac{Q^2}{2gW^2h_0^3}\frac{h_0^3}{(h_0+\Delta h)^3}\right)}{\left(1+\frac{Fr_0^2}{2}\right)} - 1 = \frac{\left(1+\frac{\Delta h}{h_0}\right)\left(1+\frac{Fr_0^2}{2}\frac{1}{\left(1+\frac{\Delta h}{h_0}\right)^3}\right)}{\left(1+\frac{Fr_0^2}{2}\right)} - 1 \qquad (A1)$$

In the domain $Fr_0 < 0.3$, $1.05 > \left(1+\frac{Fr_0^2}{2}\right) \approx 1$ and $1.05 > \left(1 + \frac{Fr_0^2}{2}\frac{1}{\left(1+\frac{\Delta h}{h_0}\right)^3}\right) \approx 1$ thus Eq. (A1) can be simplified in

$\frac{\Delta H}{H_0} \approx \frac{\Delta h}{h_0}$.

475   Conversely for $Fr_0 > 0.3$, Eq. (A1) should be used because $\frac{\Delta H}{H_0} \approx \frac{\Delta h}{h_0}$ become quite inaccurate.

Data availability

All data and more pictures are available in the report Piton et al. (2019b) from: https://hal.archives-ouvertes.fr/hal-02515247

Author contribution

GP lead the study, TH and LS performed the experiments, contributed to the analysis and reviewed the paper, SL supervised
480   the study and reviewed the paper.

Competing interests

The authors declare that they have no conflict of interest.

Acknowledgment

The authors would like to thanks Hervé Bellot, Alexis Buffet, Christian Eymond-Gris, Firmin Fontaine, Muhammad Badar
485 Munir and Frédéric Ousset for help and assistance during the preparation of this experimental campaign. This work was
funded by the French Ministry of Environment (Direction Générale de la Prévention des Risques - Ministère de la Transition
Ecologique et Solidaire) within the multi-risk agreement SRNH-IRSTEA 2019 (Action FILTOR).

References

Addy S, Wilkinson ME. 2019. Representing natural and artificial in-channel large wood in numerical hydraulic and
490 hydrological models. Wiley Interdisciplinary Reviews: Water **6** DOI: 10.1002/wat2.1389

Armanini A, Dellagiacoma F, Ferrari L. 1991. From the check dam to the development of functional check dams. Fluvial
Hydraulics of Mountain Regions **37** : 331–344. DOI: 10.1007/BFb0011200

Bezzola GR, Sigg H, Lange D. 2004. Driftwood retention works in Switzerland [Schwemmholzrückhalt in der Schweiz].
29–40 pp. [online] Available from: http://www.interpraevent.at/palm-
495 cms/upload_files/Publikationen/Tagungsbeitraege/2004_3_VII-29.pdf

Braudrick CA, Grant GE, Ishikawa Y, Ikeda H. 1997. Dynamics of Wood Transport in Streams: A Flume Experiment. Earth
Surface Processes and Landforms **22** : 669–683. DOI: 10.1002/(SICI)1096-9837(199707)22:7<669::AID-
ESP740>3.0.CO;2-L

Chen, J., Wang, D., Zhao, W. et al. Laboratory study on the characteristics of large wood and debris flow processes at slit-
500 check dams. Landslides (2020). https://doi.org/10.1007/s10346-020-01409-3

CFBR. 2013. Recommandations pour le dimensionnement des évacuateurs de crues de barrages [Dam spillway design
guidelines] . Groupe de Travail Dimensionnement des évacuateurs de crues de barrages (ed). Comité Français des Barrages
et Réservoirs [online] Available from: http://www.barrages-cfbr.eu/IMG/pdf/recommandations_cfbr_2013_evc.pdf

Comiti F, Lucıa A, Rickenmann D. 2016. Large wood recruitment and transport during large floods: A review.
505 Geomorphology **269** : 23–39. DOI: 10.1016/j.geomorph.2016.06.016

D'Agostino V, Degetto M, Righetti M. 2000. Experimental investigation on open check dam for coarse woody debris
control. In Dynamics of water and sediments in mountain basins ,. Bios; 201–212. [online] Available from:
http://intra.tesaf.unipd.it/people/dagostino/Pubblicazioni/P43_2000.pdf

Deymier C, Tacnet JM, Mathys N. 1995. Conception et calcul de barrages de correction torrentielle [Design and
510 computation of check dams] . Cemagref Grenoble Pegr

Dodge BH. 1948. Design and Operation of Debris Basins. In Proceedings, Federal Inter-Agency Sedimentation Conference
,. US Department of the Interior, Bureau of Reclamation; 274–301.

Furlan P. 2019. Blocking probability of large wood and resulting head increase at ogee crest spillways, EPFL (Lausanne)
and IST (Lisboa) [online] Available from: https://infoscience.epfl.ch/record/264198

515   Furlan P, Pfister M, Matos J, Amado C, Schleiss AJ. 2018. Experimental repetitions and blockage of large stems at ogee crested spillways with piers. Journal of Hydraulic Research **57** : 250–262. DOI: 10.1080/00221686.2018.1478897

Hartlieb A. 2012. Large scale hydraulic model tests for floating debris jams at spillways. In Water infinitely deformable but still limited. Proc. of the 2nd IAHR European Congress, ,. 1–6. [online] Available from: https://www.bgu.tum.de/fileadmin/w00blj/wb/_migrated_content_uploads/Part_C.zip

520   Hartlieb A. 2017. Decisive Parameters for Backwater Effects Caused by Floating Debris Jams. Open Journal of Fluid Dynamics **07** : 475–484. DOI: 10.4236/ojfd.2017.74032

Horiguchi T, Shibuya H, Katsuki S, Ishikawa N, Mizuyama T. 2015. A Basic Study on Protective Steel Structures against Woody Debris Hazards. International Journal of Protective Structures **6** : 191–215. DOI: 10.1260/2041-4196.6.2.191

Hübl J, Fiebiger G. 2005. Debris-flow hazards and related phenomena. In Jakob M and Hungr O (eds). Springer; 445–487.

525   Ikeya H. 1985. Study on sediment control effect of open dams. In International symposium on Erosion, Débris Flow and Disaster Prevention ,. Japan Erosion Control Engineering Society; 401–406.

Ikeya H. 1989. Debris flow and its countermeasures in Japan. Bulletin - International Association of Engineering Geology **40** : 15–33.

Ishikawa Y. 1994. Production and Flow Down of Floating Logs at Sreams and Disasters [in Japanese]. Water Science **38** :
530   51–77. DOI: 10.20820/suirikagaku.38.1_51

Ishikawa Y, Mizuyama T. 1988. An Experimental study of permeable sediment control dams as a countermeasure against floating logs. In 6th Congress Asian and Pacific Regional Division - IAHR ,. Dept. of Civil Engineering, Kyoto University; 723–730.

Kasai S, Ohgi Y, Mizoguchi I, Matsuda A, Aramaki H, Tanami M. 1996. Structural characteristics of wood-debris
535   entrapment facilites. In INTERPRAEVENT Conference Proceedings , .[online] Available from: http://www.interpraevent.at/palm-cms/upload_files/Publikationen/Tagungsbeitraege/1996_5_271.pdf

Kimura I, Kitazono K. 2019. Effects of the driftwood Richardson number and applicability of a 3D–2D model to heavy wood jamming around obstacles. Environmental Fluid Mechanics DOI: 10.1007/s10652-019-09709-6

Lange D, Bezzola G. 2006. Schwemmholz - Probleme und Lösungsansätze [Driftwood - Problems and solutions] .
540   Versuchsanstalt für Wasserbau Hydrologie und Glaziologie der Eidgenössischen Technischen Hochschule (VAW) Zürich [online] Available from: https://ethz.ch/content/dam/ethz/special-interest/baug/vaw/vaw-dam/documents/das-institut/mitteilungen/2000-2009/188.pdf

Mazzorana B, Fuchs S. 2010. Fuzzy Formative Scenario Analysis for woody material transport related risks in mountain torrents. Environmental Modelling & Software **25** : 1208–1224. DOI: 10.1016/j.envsoft.2010.03.030

545   Mazzorana B, Zischg A, Largiader A, Hübl J. 2009. Hazard index maps for woody material recruitment and transport in alpine catchments. Natural Hazards and Earth System Science **9** : 197–209. DOI: 10.5194/nhess-9-197-2009

Meninno S, Canelas RB, Cardoso AH. 2019. Coupling check dams with large wood retention structures in clean water. Environmental Fluid Mechanics DOI: 10.1007/s10652-019-09711-y

Merten E, Finlay J, Johnson L, Newman R, Stefan H, Vondracek B. 2010. Factors influencing wood mobilization in streams.
550   Water Resources Research **46** DOI: 10.1029/2009wr008772

Mizuyama T. 2008. Structure Contermeasures for Debris Flow Disasters. International Journal of Erosion Control
Engineering, Vol.1, No.2, DOI: 10.13101/ijece.1.38

Pfister M, Capobianco D, Tullis B, Schleiss AJ. 2013a. Debris-Blocking Sensitivity of Piano Key Weirs under Reservoir-
Type Approach Flow. Journal of Hydraulic Engineering **139** : 1134–1141. DOI: 10.1061/(asce)hy.1943-7900.0000780

555   Pfister M, Schleiss AJ, Tullis B. 2013b. Effect of driftwood on hydraulic head of Piano Key weirs. In Labyrinth and Piano
Key weirs II ,. CRC Press/Balkema Leiden, Netherlands; 255–264.

Piton G, Carladous S, Marco O, Richard D, Liebault F, Recking A, Quefféléan Y, Tacnet JM. 2019a. Usage des ouvrages de
correction torrentielle et plages de dépôt : origine, état des lieux, perspectives. La Houille Blanche : 57–67. DOI:
10.1051/lhb/2019008

560   Piton G, Marchal L, Lambert S. 2019b. Etude des interactions barrages filtrants / transport de flottants et risque de relargage
- étude expérimentale des ouvrages rigides [Interactions between open check dams and large wood and overtopping hazards
- experimental study of rigid barriers] . IRSTEA Grenoble ; DGPR (Direction Générale de la Prévention des Risques -
Ministère de la Transition Ecologique et Solidaire) [online] Available from: https://hal.archives-ouvertes.fr/hal-02515247

Piton G, Mejean S, Bellot H, Le Guern J, Carbonari C, Recking A. 2016. Bed-load trapping in open check dam basins
565   measurments of flow velocities and depositions patterns. In INTERPRAEVENT Conference proceedings , Koboltschnig G
(ed). International Research Society INTERPRAEVENT: Klagenfurt (Austria); 808–817. [online] Available from:
http://www.interpraevent.at/palm-cms/upload_files/Publikationen/Tagungsbeitraege/2016_1_808.pdf

Piton G, Recking A. 2016a. Design of sediment traps with open check dams. I: hydraulic and deposition processes. Journal
of Hydraulic Engineering **142** : 1–23. DOI: 10.1061/(ASCE)HY.1943-7900.0001048

570   Piton G, Recking A. 2016b. Design of sediment traps with open check dams. II: woody debris. Journal of Hydraulic
Engineering **142** : 1–17. DOI: 10.1061/(ASCE)HY.1943-7900.0001049

Reneuve P. 1955. L'évolution de la technique de correction torrentielle. Revue Forestière Française : 689–693. DOI:
10.4267/2042/27132

Rossi G, Armanini A. 2019. Experimental analysis of open check dams and protection bars against debris flows and
575   driftwood. Environmental Fluid Mechanics DOI: 10.1007/s10652-019-09714-9

Rudolf-Miklau F, Suda J. 2013. Design Criteria for Torrential Barriers. In Dating Torrential Processes on Fans and Cones ,
Schneuwly-Bollschweiler M, Stoffel M, and Rudolf-Miklau F (eds). Springer Netherlands; 375–389.

Ruiz-Villanueva V et al. 2019. Characterization of wood-laden flows in rivers. Earth Surface Processes and Landforms DOI:
10.1002/esp.4603

580   Ruiz-Villanueva V, Bladé E, Sánchez-Juny M, Marti-Cardona B, Dıez-Herrero A, Bodoque JM. 2014a. Two-dimensional
numerical modeling of wood transport. Journal of Hydroinformatics **16** : 1077. DOI: 10.2166/hydro.2014.026

Ruiz-Villanueva V, Bodoque JM, Dıez-Herrero A, Bladé E. 2014b. Large wood transport as significant influence on flood
risk in a mountain village. Natural Hazards **74** : 967–987. DOI: 10.1007/s11069-014-1222-4

SABO Division. 2000. Guideline for driftwood countermeasures (proposal and design) . Department SC (Sabo) (ed).
585 Ministry of Construction. Japan. [online] Available from: http://www.sabo-int.org/guideline/pdf/driftwoodCountermeasureGuideline.pdf

Schalko I, Lageder C, Schmocker L, Weitbrecht V, Boes RM. 2019a. Laboratory flume experiments on the formation of spanwise large wood accumulations Part I: Effect on backwater rise. Water Resources Research DOI: 10.1029/2018wr024649

590 Schalko I, Lageder C, Schmocker L, Weitbrecht V, Boes RM. 2019b. Laboratory flume experiments on the formation of spanwise large wood accumulations Part II: Effect on local scour. Water Resources Research DOI: 10.1029/2019WR024789

Schalko I, Schmocker L, Weitbrecht V, Boes RM. 2018. Backwater Rise due to Large Wood Accumulations. Journal of Hydraulic Engineering **144** : 04018056. DOI: 10.1061/(asce)hy.1943-7900.0001501

Schmocker L, Hager WH. 2013. Scale modeling of wooden debris accumulation at a debris rack. Journal of Hydraulic
595 Engineering **139** : 827–836. DOI: 10.1061/(ASCE)HY.1943-7900.0000714

Schmocker L, Hunziker R, Müller U, Weitbrecht V. 2014. Driftwood retention in pre-alpine rivers. In Proceedings of the 7th International Conf. on Fluvial Hydraulics, RIVER FLOW ,. CRC Press/Balkema; 117–127.

Schmocker L, Weitbrecht V. 2013. Driftwood: Risk analysis and engineering measures. Journal of Hydraulic Engineering **139** : 683–695. DOI: 10.1061/(ASCE)HY.1943-7900.0000728

600 Shima J, Moriyama H, Kokuryo H, Ishikawa N, Mizuyama T. 2016. Prevention and mitigation of debris flow hazards by using steel open-type sabo dams. International Journal of Erosion Control Engineering **9** : 135–144. DOI: 10.13101/ijece.9.135

Shima J, Yoshida K, Kawakami Y, Mizuyama T. 2015. Consideration on boulders & members' interval of open type steel sabo dam for capturing debris flow. Journal of the Japan Society of Erosion Control Engineering **67** DOI:
605 10.11475/sabo.67.5_3

Shrestha BB, Nakagawa H, Kawaike K, Baba Y, Zhang H. 2012. Driftwood deposition from debris flows at slit-check dams and fans. Natural Hazards **61** : 577–602. DOI: 10.1007/s11069-011-9939-9

Di Stefano C, Ferro V. 2013. Experimental study of the stage-discharge relationship for an upstream inclined grid with longitudinal bars. Journal of Irrigation and Drainage Engineering **139** : 691–695. DOI: 10.1061/(ASCE)IR.1943-
610 4774.0000598

Stockstill RL, Daly SF, Hopkins MA. 2009. Modeling Floating Objects at River Structures. Journal of Hydraulic Engineering **135** : 403–414. DOI: 10.1061/(asce)0733-9429(2009)135:5(403)

Uchiogi T, Shima J, Tajima H, Ishikawa Y. 1996. Design methodes for woody-debris entrapment. In INTERPRAEVENT Conference Proceedings ,. International Research Society INTERPRAEVENT; 279–288. [online] Available from:
615 http://www.interpraevent.at/palm-cms/upload_files/Publikationen/Tagungsbeitraege/1996_5_279.pdf

Wickham H. 2016. ggplot2: Elegant Graphics for Data Analysis . Springer-Verlag New York [online] Available from: https://ggplot2.tidyverse.org

Wohl E et al. 2019. The Natural Wood Regime in Rivers. BioScience **69** : 259–273. DOI: 10.1093/biosci/biz013

Wohl E, Bledsoe BP, Fausch KD, Kramer N, Bestgen KR, Gooseff MN. 2016. Management of Large Wood in Streams: An
620   Overview and Proposed Framework for Hazard Evaluation. JAWRA Journal of the American Water Resources Association
52 : 1–21. DOI: 10.1111/1752-1688.12388

Zollinger F. 1985. Debris detention basins in the European Alps. In International symposium on Erosion, Debris Flow and
Disaster Prevention. Japan Erosion Control Engineering Society; 433–438.